magnetochemistry

MDPI

Article

Strong Antiferromagnetic Interactions in the Binuclear Cobalt(II) Complex with a Bridged Nitroxide Diradical

Vitaly A. Morozov [1], Eugenia V. Peresypkina [2], Wolfgang Wernsdorfer [3] and Kira E. Vostrikova [4,*]

1 International Tomography Center SB RAS, Institutskaya Str. 3a, 630090 Novosibirsk, Russia; moroz@tomo.nsc.ru
2 Institut für Anorganische und Analytische Chemie, Goethe-Universität Frankfurt am Main, Max-von-Laue-Straße 7, 60438 Frankfurt am Main, Germany; eugeniaperesypkina@gmail.com
3 Physikalisches Institut, Karlsruhe Institute of Technology, 76131 Karlsruhe, Germany; wolfgang.wernsdorfer@kit.edu
4 Nikolayev Institute of Inorganic Chemistry SB RAS, 3 Lavrentiev Avenue, 630090 Novosibirsk, Russia
* Correspondence: vosk@niic.nsc.ru

Abstract: A binuclear cobalt–radical complex formed by the reaction of $Co(hfac)_2 \cdot 2H_2O$ (hfac = hexafluoroacetylacetonate) with the 2,2-bis(1-oxyl-3-oxide-4,4,5,5-tetramethylimidazolinyl) biradical (BR) has been synthesized. The complex $\{(hfac)Co^{II}(BN)Co^{II}(hfac)\}$ crystallizes in the triclinic space group $P\bar{1}$: $C_{34}H_{28}Co_2F_{24}N_4O_{12}$, a = 11.1513(5) Å, b = 12.8362(7) Å, c = 18.2903(8) Å, α = 103.061(1)°, β = 100.898(2)°, γ = 102.250(1)°, Z = 2. The compound consists of two non-equivalent pseudo-octahedral Co^{II} ions, each bearing *two hfac* ancillary ligands bridged by the tetradentate bis-nitroxide (BN). The temperature dependence of the magnetic susceptibility indicates a strong antiferromagnetic exchange between each of the Co^{2+} ions and the nitroxyl biradical, as well as between the spins within the bridging ligand, forming a spin-frustrated system. Micro-squid investigations, performed on a single crystal of $\{(hfac)Co^{II}(BN)Co^{II}(hfac)\}$, reveal a peculiarity of the M(H) graph at temperatures below 0.4 K displaying a step that is a result of ground and first excited levels mixing by the applied magnetic field due to a small energy gap between them, as inferred from ab initio calculation. The latter was also carried out for two models of mononuclear Co^{2+} complexes in order to obtain a set of initial parameters for fitting the experimental magnetic curves using the Phi program. Moreover, direct CAS(12,10)/def2-TZVP calculations of the magnetic dependences χT(T) and M(H) were performed, which satisfactorily reproduced the experimental ones.

Keywords: nitroxyl radical; diradical; cobalt(II) complex; strong magnetic coupling; spin frustration

Citation: Morozov, V.A.; Peresypkina, E.V.; Wernsdorfer, W.; Vostrikova, K.E. Strong Antiferromagnetic Interactions in the Binuclear Cobalt(II) Complex with a Bridged Nitroxide Diradical. *Magnetochemistry* **2024**, *10*, 82. https://doi.org/10.3390/magnetochemistry10110082

Academic Editor: Gordon T. Yee

Received: 19 September 2024
Revised: 20 October 2024
Accepted: 24 October 2024
Published: 28 October 2024

1. Introduction

Among the various strategies developed to create magnetic systems, the metal–radical approach has yielded successful results. This approach, proposed by Andrea Caneschi, Dante Gatteschi, Roberta Sessoli, and Paul Rey [1], aims at obtaining strong direct magnetic metal–ligand exchange interactions by coordinating paramagnetic metal ions with stable free radicals. Such a strategy has been employed to obtain magnetic systems with incredibly strong couplings. In some cases, the interaction can propagate in one, two, or even three directions [2], giving rise to molecular systems with cooperative magnetic behavior [3–7]. The presence of strong exchange interactions between metal ions and organic radicals in coordination compounds makes them attractive for the design of molecular magnetic materials [8,9]. This is especially true for the low-dimensional magnets: single-molecule magnets (SMMs) [10] and single-chain magnets (SCMs) [11–13] since the stronger the spin coupling, the lower the under-barrier magnetization tunneling [14,15].

Antiferromagnetically coupled spins in polynuclear complexes of paramagnetic metal ions [16] and π-conjugated organic radicals [3,17] can be organized in different topological forms: triangular [18]; butterfly-like [13,19–21]; tetrahedral; or cubane structures. Therefore,

such materials offer plentiful opportunities to describe competing interactions, where two adjacent spins are forced to be parallel despite antiferromagnetic coupling. A molecule with a degenerate ground state is called spin-frustrated. The versatility of molecular magnetic materials could be greatly improved by the use of heterospin systems consisting of paramagnetic metal ions in combination with organic free radical bridging ligands [22–26].

Among the 3d metals, coordination compounds of Mn(II) with stable organic radicals are of most interest due to the presence of five unpaired electrons in the metal cation. However, the Mn^{2+} ion is magnetically isotropic, whereas the Co^{2+} ion is anisotropic in an idealized octahedral environment due to the partially unquenched orbital moment L [27]. In the family of organic radicals, most of which are unstable in the air [17,28,29], the nitronyl nitroxide radicals 2-(S)-4,4,5,5-tetramethyl-4,5-dihydro-1H-imidazol-1-oxy-3-oxide (NNS), where S is a substituent, are the most extensively used due to their outstanding persistence, ease of chemical modification, and ability to perform a bridging function linking two metal ions [30–32]. As ligands, NNRs are weak donors owing to their weak Lewis-base nature. In order to promote coordination, strong electron-withdrawing groups, such as the *hfac* anion (*hfac* = hexafluoroacetylacetonato), are employed to increase the acidity of a metallic ion.

The diradical 2,2′-bis(1-oxyl-3-oxide-4,4,5,5-tetramethyl-imidazolinyl) (BN) (Scheme 1), which was first described by Ullman et al. [33] and thereafter, fully examined magnetically by Paul Rey et al. [34]. They found that the spins of the monoradicals in BN are strongly coupled with an exchange constant $2J_1 = –311$ cm^{-1}. Further, BN was used to synthesize a Ni^{2+} compound [35], representing a mononuclear complex of the bidentate chelating radical BN $[Ni_2(hfac)_4(BN)(H_2O)_2]$ hydrogen-bonded to the $[Ni^{II}(hfac)_2(H_2O)_2]$ moiety [35] ($J_2 = J_3 = -236.3$ cm^{-1}), as well as a binuclear complex $[(hfac)Mn^{II}(BN)Mn^{II}(hfac)]$ with bis-bidentate BN [36]. Since then, no coordination compounds of other transition metals with BN have been described. Herein, we report the synthesis and characterization of a new binuclear complex of bridging bischelate diradical BN, representing a spin-frustrated system consisting of cobalt(II) bis(hexafluoroacetylacetonate) and BN. A butterfly-like spin arrangement was found in this binuclear system.

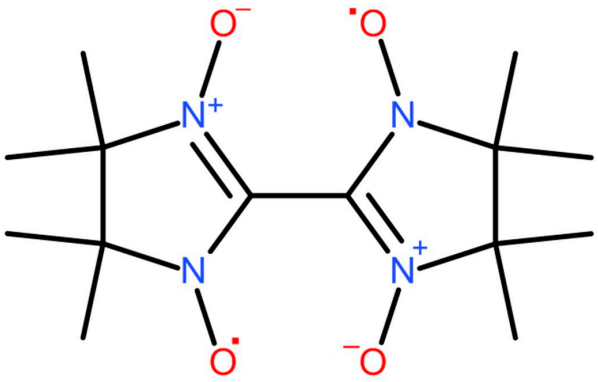

Scheme 1. The diradical 2,2′-bis(1-oxyl-3-oxide-4,4,5,5-tetramethyl-imidazolinyl) (BN).

2. Materials and Methods

2.1. Instrumental and Physical Measurements

Elemental (C,H,N) analysis was performed on a Euro-Vector 3000 analyzer (Eurovector, Redavalle, Italy). FTIR spectra were registered with a NICOLET spectrophotometer (Thermo Electron Scientific Instruments LLC, Madison, WI, USA) in the 4000–400 cm^{-1} range. Powder X-ray diffraction (PXRD) measurements were conducted at room temperature using Cu-Kα radiation (λ = 1.5418 Å) on a Shimadzu XRD-7000 diffractometer (Shimadzu, Kyoto, Japan). The magnetic properties of the compound were studied using a Quantum Design MPMS 5XL SQUID magnetometer (Quantum Design, Inc., San Diego, CA, USA) in the temperature range of 1.8–300 K and under a magnetic field of up to 50 kOe. The magnetic susceptibility was corrected for the diamagnetic contribution calculated from

Pascal's constants [37]. Ultra-low temperature (>1.8 K) magnetization measurements on single crystals were performed using a μ-SQUID array [38].

Single-crystal XRD experimental details are presented in Table S1 (Supplementary Materials). Crystallographic data were deposited with the Cambridge Crystallographic Data Centre (deposit number CCDC 2366221).

2.2. Theoretical Calculations

Quantum chemical study was fulfilled using crystallographic geometry. Magnetic exchange *J* integrals calculations by both broken-symmetry [39] DFT (BS-DFT) and ab initio CAS/NEVPT2 methods with def2-TZVP basis and def2-TZVPP basis set for Co were performed by means of the ORCA-6.0 software package [40,41]. Fitting of the experimental χT(T) and *M*(H) dependences to obtain optimal parameters of employed spin–Hamiltonian was carried out using the PHI 3.16 package [42].

2.3. Preparations

Solvents of the reagent grade (EKOS-1, Moscow, Russia) were distilled prior to use. The complex was synthesized under ambient conditions. The diradical 2,2′-bis(1-oxyl-3-oxide-4,4,5,5-tetramethyl-imidazolinyl) (BN) was synthesized according to a literature procedure [34].

Synthesis of $\{(hfac)_2Co^{II}(BN)Co^{II}(hfac)_2\}$

A powder of $[Co(hfac)_2(H_2O)_2]\cdot 2H_2O$ [43] (54.5 mg, 0.05 mmol) was stirred in *n*-heptane (30 mL) at boiling until the volume of the solution was reduced by half to remove H_2O by means of azeotrope formation. A diradical (8 mg, 0.025 mmol) solution in methylene chloride (5 mL) was added to the warm heptane solution of $[Co(hfac)_2]$. The dark brown reaction mixture was stirred at ~40 °C to partially remove CH_2Cl_2 and then filtered into a vial of a suitable volume. The vial was tightly closed with a white rubber stopper and placed in a dark place. After a few days, due to the slow pumping of the CH_2Cl_2 vapors through a stopper material, most of the complex crystallized, and it was decanted by removing the slightly colored mother liquor. The dark crystals were rinsed with a small amount of heptane and air-dried. Visual examination of the crystalline sample under a microscope revealed its high homogeneity. Yield 31.5 mg (95%) Anal Calcd. for $C_{34}H_{28}Co_2F_{24}N_4O_{12}$ (mass. %): C, 32.43; H, 2.24; N, 4.45; found: C, 32.52; H, 2.2; N, 4.5. IR spectrum (KBr, ν, cm^{-1}): 1260, 1655, 3005.

3. Results and Discussion

3.1. Synthesis and Characterization

It should be noted that for the synthesis of $\{(hfac)_2Co^{II}(BN)Co^{II}(hfac)_2\}$, we applied a general approach commonly used for complexes of metal hexafluoroacetylacetonates with nitronyl nitroxides, requiring recrystallization of the final product obtained as powder from heptane–CH_2Cl_2 solution. However, we were able to avoid the second step, recrystallization, by finding conditions for a slow evaporation of the mother liquor. A simple tool, a white rubber stopper, was used to slowly absorb the remaining dichloromethane from the reaction mixture. This allowed to obtain the substance in the form of nicely faceted crystals without any admixture of starting products. Such a method of synthesis yields in a pure complex using small amounts of the precursors. Since our complex turned out to be isostructural to the previously studied manganese analog [36], its IR spectrum is very close to the latter.

The composition of the main fraction of the complex was confirmed by elemental analysis, and its phase purity was proved by powder X-ray diffraction patterns presented in Figure S1.

3.2. Crystal and Molecular Structure

The crystal and molecular structure of the complex (Figure 1) was determined by single-crystal X-ray diffraction (SCXRD). As for the Mn congener, the complex molecular structure of BN in $\{(hfac)_2Co^{II}(BN)Co^{II}(hfac)_2\}$ is very close to that stated for the free diradical [34]. The length of the C—C bond between the two five-membered heterocycles of 1.452(4) Å is almost the same as for the free ligand (1.439(3) Å, considering the temperature difference in the X-ray diffraction experiment). The dihedral angles between the two nitronyl nitroxide radical planes in the complex are ~53°, which are slightly smaller than those in uncoordinated BN [34]. These similarities suggest that the diradical ligand forms the binuclear complex with little structural variation. This implies that the magnetic interaction between the two radical centers in BN should be minimally altered by complexation. It should be emphasized that cobalt ions have a non-equivalent pseudo-octahedral environment, with the equatorial octahedron's planes being practically perpendicular to each other, with a plane-to-plane twist angle of 92.35°.

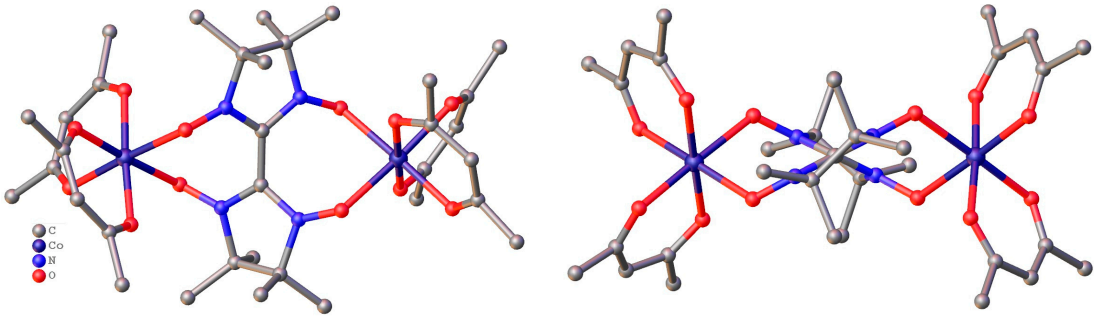

(**a**) (**b**)

Figure 1. Molecular structure of the complex–H and F atoms are omitted for clarity: (**a**) front view; (**b**) side-view demonstrating the twisting of two five-membered heterocycles in a diradical moiety.

3.3. Magnetic Studies

3.3.1. SQUID Magnetometry at 2–300 K

The temperature dependence of susceptibility for a randomly oriented polycrystalline sample of the complex is presented in Figure 2 as a χT vs. T plot. From room temperature up to 200 K, the χT value varies slightly around ~3.3 emu K mol^{-1}. This value is much lower than the value of χT = 4.5 emu K mol^{-1} for non-interacting spins in the high-spin octahedral Co(II) complex with averaged g = 2 (2 × 1.875 emu K mol^{-1} for two Co^{2+} with S = 3/2 and 2 × 0.375 for two spins of 1/2 for two noninterected nitronyl nitroxides). However, assuming that all spins are involved in a strong antiferromagnetic coupling so that the resulting spin of the complex could be equal to 2, then χT (g = 2) should be equal to 3.0 emu K mol^{-1}, which is close to the experimental value. Further, the plot decreases, reaching 1.6 emu K mol^{-1} at 2 K.

To probe the spin value of the magnetic system ground state, the field dependence of the magnetization was studied at a temperature of 2 K (see Figure 3). At the field of 5 T, the magnetization value of 3.05 μ_B demonstrates that M(H) does not really reach a saturation value of ~4 μ_B, as expected for four unpaired electrons. Such a low value at H = 5 T may indicate both the presence of strong antiferromagnetic interactions and the manifestation of magnetic anisotropy associated with spin–orbit coupling in Co centers. These results are in agreement with the literature data for the Co-NIT systems [9,11,20,21,27,44,45].

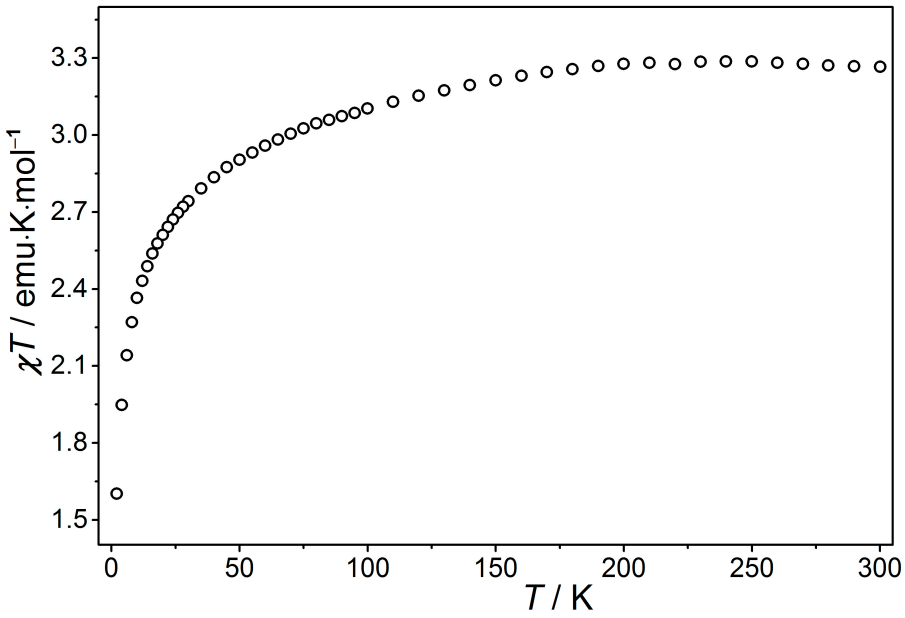

Figure 2. Temperature dependence of χT product at H = 0.1 T.

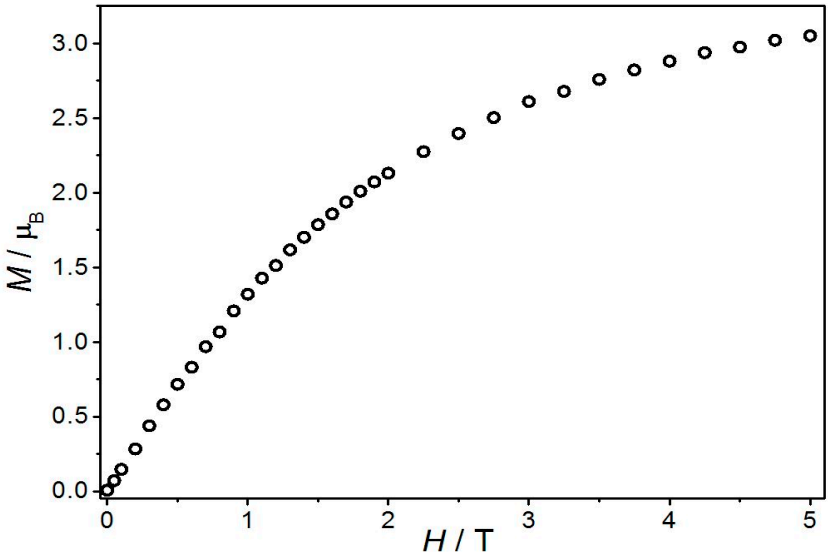

Figure 3. Magnetization curve measured at 2.8 K.

3.3.2. Micro-SQUID Magnetic Measurements at Extremely Low Temperatures

By means of an in-house-made μ-SQUID system, additional M versus H data down to 30 mK (Figures 4 and S2) have been collected from single crystals. As shown in Figure 4 for $\{(hfac)_2Co^{II}(BN)Co^{II}(hfac)_2\}$, the M/M_s (M_s is a saturation field) versus H magnetization curves have no hysteresis below 1.4 K (Figure S2). An interesting feature of the M(H) plot at temperatures below 0.4 K (Figures 4 and S2) is the presence of a step, which, according to the ab initio calculations performed and discussed below, correlates with the energy gap of 0.69 cm^{-1} (Table S2) between the main and the first excited singlet levels. Their mixing by the applied magnetic field determines exactly this shape of the magnetization plot.

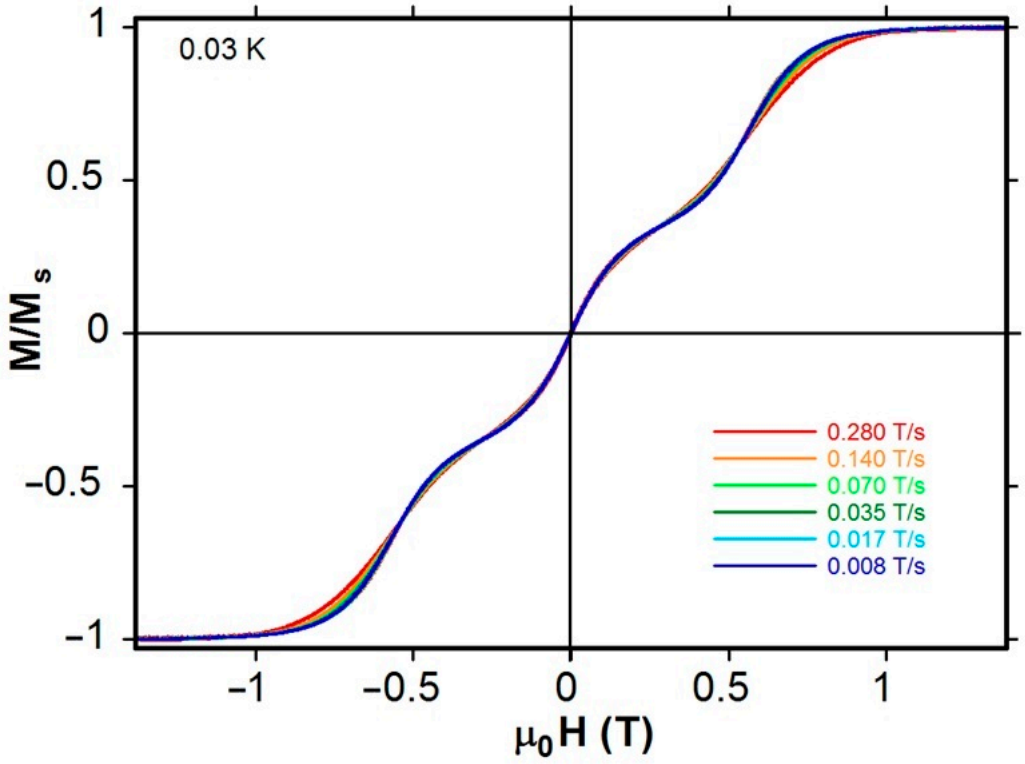

Figure 4. Field dependences of the normalized magnetization measured at different sweep rates at 0.03 K from a single crystal of {(hfac)$_2$Co^{II}(BN)Co^{II}(hfac)$_2$}.

3.4. Magnetic Behavior Modeling and Theoretical Calculations

3.4.1. Theoretical Model and Exhaustive Parameter Set Required for Magnetic Data Simulation

The studied dimeric complex of cobalt is a rather complex system in magnetic terms. This is due to the fact that the modeling of its magnetic behavior requires a set of numerous parameters that must be varied during the fitting. In addition to the set of magnetic exchange interactions (*J*) shown in Scheme 2, other parameters for describing the magnetic contributions of the metal centers are needed to accurately describe the system consisting of two high-spin Co^{2+} ions in a non-equivalent pseudo-octahedral coordination environment. These include the spin–orbit coupling parameter, λ, two parameters, $B_2^{(0)}$ and $B_2^{(2)}$, describing the octahedral crystal field, and in the case of non-equivalent Co^{2+} ions, each of them requires a double set of these parameters.

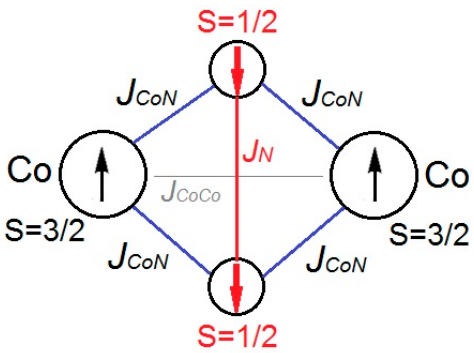

Scheme 2. Magnetic exchange interactions in complex {(hfac)$_2$Co^{II}(BN)Co^{II}(hfac)$_2$}.

In addition, as mentioned in the description of the molecular structure of {(hfac)$_2$Co^{II}(BN)Co^{II}(hfac)$_2$}, the local coordinate axes of the two coordination polyhedra are not parallel. Since the bridging biradical is not planar, mirror symmetry is not realized in this butterfly-like molecule because the equatorial planes of the two octahedrons

are practically perpendicular to each other. Consequently, in order to bring the coordination environments for both Co centers to a common molecular coordinate system, it is necessary to perform the unitary transformation from the molecular coordinate system to the local ones [46,47]. However, the latter would not be accurate due to the mismatch of bond lengths and angles between the corresponding bonds for Co1 and Co2. Moreover, the use of the set of variables consisting of the two crystal field parameters and one spin–orbit coupling parameter per each cobalt ion will contribute to overparameterization. For the same purpose, we do not take into account the Co–Co superexchange interaction since it should be much smaller than J_N and J_{CoN}, as it usually does not exceed 10 cm^{-1} for the studied cobalt (II) compounds [48–52].

3.4.2. Description of Spin–Hamiltonians Used in Theoretical Calculations

The following spin–Hamiltonian was used to find the magnetic exchange coupling constant, J_N, in the bridging diradical BN.

$$\hat{H} = -2J_N\,\hat{S}_{N1}\cdot\hat{S}_{N2} \quad (1)$$

To describe the Co^{2+} spin system, we used the Griffith Hamiltonian [53,54] $\boldsymbol{H}^{Co}$, which takes into account the spin–orbit interaction of S = 3/2 with the fictitious orbital triplet $L = 1$ and the octahedral crystal field Hamiltonian $\boldsymbol{H}_{CF}^{Co}$ of the Co^{2+} ion, containing the orbital spin operators $\boldsymbol{O}_2^0$ and $\boldsymbol{O}_2^2$:

$$\boldsymbol{H}^{Co} = \lambda\boldsymbol{S}\cdot\sigma\boldsymbol{L} + \boldsymbol{H}_{CF}^{Co} \quad (2)$$

$$\boldsymbol{H}_{CF}^{Co} = \sigma^2\left(B_2^{(0)}\boldsymbol{O}_2^0 + B_2^{(2)}\boldsymbol{O}_2^2\right);\boldsymbol{O}_2^0 = 3\boldsymbol{L}_z^2 - \boldsymbol{L}^2;\boldsymbol{O}_2^2 = {}^1/_2\left(\boldsymbol{L}_+^2 - \boldsymbol{L}_-^2\right) \quad (3)$$

Unlike a true orbital momentum, the fictitious orbital angular momentum $L = 1$ enters all expressions in the Griffith Hamiltonians in combination with the orbital reduction factor $\sigma = -3/2\kappa$, where κ is the so-called covalence parameter ($0 < \kappa < 1$), which is assumed to be equal to 1 for an isolated Co^{2+} ion. In the literature [55], other designations for the crystal field parameters are sometimes used: $\Delta_{ax} = 3B_2{}^{(0)}\sigma^2$—the axial field parameter, and $\Delta_{rh} = B_2{}^{(2)}\sigma^2$—the rhombic field parameter.

The full spin–Hamiltonian for the complex $\{(hfac)_2Co^{II}(BN)Co^{II}(hfac)_2\}$ can then be represented as

$$\boldsymbol{H} = \boldsymbol{H}^{Co1} - 2J_{CoN}\boldsymbol{S}_{Co1}\cdot(\boldsymbol{S}_{N1} + \boldsymbol{S}_{N2}) + \boldsymbol{H}^{Co2} - 2J_{CoN}\boldsymbol{S}_{Co2}\cdot(\boldsymbol{S}_{N1} + \boldsymbol{S}_{N2})\cdot 2J_N\boldsymbol{S}_{N1}\cdot\boldsymbol{S}_{N2} \quad (4)$$

where $\boldsymbol{H}^{Co1}$ and $\boldsymbol{H}^{Co2}$ are the Griffith spin–Hamiltonians (2) of Co ions; J_{CoN} is the exchange integral of the interaction of Co^{2+} ions with the total spin of BN; J_N is the exchange integral of the interaction between spins in BN. Strictly speaking, the exchange integrals J_{CoN} between different pairs of Co^{2+} and BN may differ, as well as the geometric parameters of the crystal field of two Co^{2+} ions. However, this aspect is neglected in this paper.

3.4.3. Estimation of the Exchange Integral J_N

To estimate the value of the magnetic exchange interaction (J_N) between the spins in BN, quantum chemical DFT calculations were performed for the biradical fragment, preserving its geometry from the complex crystal structure. The results of the broken symmetry (BS) DFT calculations of the exchange integrals using the spin–Hamiltonian (1) are summarized in Table 1.

Table 1. $2J_N$ value for the BN-fragment calculated with def2-TZVP DFT basis sets.

DFT Level	TPSSh	B3LYP	LC-BLYP	wB97m-v	cam-B3LYP
J_N, cm^{-1}	−334	−419	−727	−732	−790

It is obvious that the obtained J_N values are somewhat overestimated in comparison with those previously found for the free BN [34] ($J = -155$ cm^{-1}) and the Mn(II) binuclear

complex ($J = -283$ cm^{-1}) [36], where the BN performs a bridging function. To refine the J_N values, an ab initio calculation of the lowest singlet–triplet gap G was performed using the CASSCF/NEVPT2 method on the def2-TZVP basis. According to the spin–Hamiltonian (1) $G = 2J_N$. The obtained J_N values are listed in Table 2.

Table 2. J_N values for the BN-fragment obtained by means of CASSCF using def2-TZVP basis sets.

CAS/Multiplets/Roots	J_{CAS}, cm^{-1}	$J_{CAS/NEVPT2}$, cm^{-1}
(10,8)/(3,1)/(10,10)	−282	−227
(14,10)/(3,1)/(10,10)	−272	−228

3.4.4. Initial Parameters Calculation for Fitting Experimental Magnetic Data Using Model Molecular Complexes

For the studied binuclear complex with four paramagnetic centers, the spin–Hamiltonian (4) requires the determination of six parameters: $\lambda; B_2^{(0)}; B_2^{(2)}; \sigma; J_{CoN}; J_{Co}$. To obtain a preliminary estimate of these parameters, a series of CASSCF/NEVPT2 calculations were performed for model complexes with a smaller number of spins. In the first step, a bischelate fragment of Co(hfac)$_2$ was excluded from the binuclear complex, and in both coordinated nitroxyl groups of BN, the nitrogen atom was replaced by a carbon atom while keeping the geometric parameters. Such a technique was used to obtain a model mononuclear complex [(hfac)$_2$Co(DD)], where DD is a diamagnetic analog of BN (Figure 5, left).

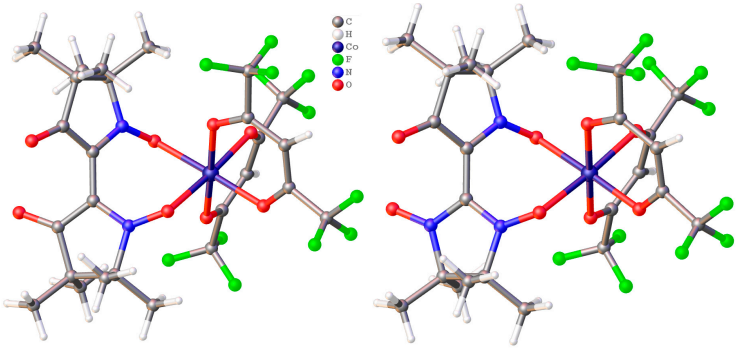

Figure 5. Mononuclear model complexes with a diamagnetic [(hfac)$_2$Co(DD)] (**left**) and monoradical [(hfac)$_2$Co(DP)] (**right**) analogs of BN.

For the [(hfac)$_2$Co(DD)] complex, a CAS(7,5)/QDPT-NEVPT2 calculation of 10 quartets and 40 doublets was performed. In addition, an analysis was performed on the resulting set of 12 levels corresponding to the splitting of the lowest Co^{2+} multiplet $^4T_{1g}$. A simulation of the relative arrangement of all 12 levels at the fixed value $\lambda = -180$ cm^{-1} yielded two optimal sets of crystal field parameters in cm^{-1}: $B_2^{(0)} = 293$, $B_2^{(2)} = -173$ and $B_2^{(0)} = -302$, $B_2^{(2)} = -11$, with almost the same approximation quality for both sets.

In the second step, for further refinement of the spin–Hamiltonian parameters, a model complex [(hfac)$_2$Co(DP)] (Figure 5, right) with two paramagnetic centers was used. This was achieved by replacing a nitrogen atom with a carbon atom in only one uncoordinated N-O group. This was performed to estimate the exchange interaction between the Co^{2+} ion and a monoradical species. For [(hfac)$_2$Co(DP)], the interaction of the lowest Co^{2+} multiplet $^4T_{1g}$ and a spin doublet of DP results in 24 levels, for which CAS(10,8)/NEVPT2 calculation was performed, finding a total of 7 quintets, 10 triplets, and 5 singlets. Then, using the spin–Hamiltonian $\boldsymbol{H} = \boldsymbol{H}^{Co} - 2J_{CoN}\boldsymbol{S}_{Co}\cdot\boldsymbol{S}_N$, where $\boldsymbol{H}^{Co}$ was taken from Equation (2), a fitting of the obtained 24 levels at a fixed $\lambda = -180$ cm^{-1} was carried out, yielding the following parameters (in cm^{-1}): $B_2^{(0)} = 293$, $B_2^{(2)} = -173$, $J_{CoN} = -53$ and $B_2^{(0)} = -302$, $B_2^{(2)} = -11$, $J_{CoN} = -95$. The quality of the approximation for these two sets differs slightly in favor of the case where $B_2^{(0)} > 0$.

The final analytical step of the model complexes was the study of a mononuclear complex [(hfac)$_2$Co(BN)] involving three paramagnetic centers: Co^{2+} and two NN radicals of BN. In this case, the interaction of the Co^{2+} ion multiplet $^4T_{1g}$ and two spin doublets of single nitroxyl radicals of BN results in low 48 levels, according to a CASSCF/NEVPT2 calculation. The latter was performed using the CAS(11,8)/NEVPT2 procedure with a total of 6 sextets, 14 quartets, and 8 doublets found. Then, at $\lambda = -180$ cm^{-1}, the fitting of the obtained 48 levels was carried out using the spin–Hamiltonian, taking into account the two exchange interactions: $\boldsymbol{H} = \boldsymbol{H}^{Co} - 2J_{CoN}\boldsymbol{S}_{Co}(\boldsymbol{S}_{N1} + \boldsymbol{S}_{N2}) - 2J_N\boldsymbol{S}_{N1}\cdot\boldsymbol{S}_{N2}$, where $\boldsymbol{H}^{Co}$ corresponds to Hamiltonian (2), giving the next two sets of parameter values (in cm^{-1}):

Set 1 – $B_2^{(0)} = 293$, $B_2^{(2)} = -173$, $J_{CoN} = -31$, $J_N = -122$;
Set 2 – $B_2^{(0)} = -302$, $B_2^{(2)} = -11$, $J_{CoN} = -54$; $J_N = -186$.

Note that the approximation accuracy for the positions of the obtained levels was higher for the parameter set with $B_2^{(0)} > 0$. For greater clarity, all parameters obtained during the calculation of the model complexes are summarized in Table 3.

Table 3. The sets of Hamiltonian parameters (in cm^{-1}) calculated at a fixed value of $\lambda = -180$ cm^{-1}.

Complex	Data Set	$B_2^{(0)}$	$B_2^{(2)}$	J_{CoN}	J_N	σ [1]	zJ
[(hfac)$_2$Co(DD)]	1	293	−173				
	2	−302	−11				
[(hfac)$_2$Co(DP)]	1	293	−173	−53			
	2	−302	−11	−95			
[(hfac)$_2$Co(BN)]	1	293	−173	−31	−122		
	2	−302	−11	−54	−186		
[(hfac)$_4$Co$_2$(BN)]	1	322	−126	−47	−125	0.07	−0.011
	2	−380	−13	−68	−203	0.07	−0.019

[1] Orbital reduction factor is a dimensionless quantity.

3.4.5. Experimental Magnetic Data Simulations for {(hfac)$_2$Co^{II}(BN)Co^{II}(hfac)$_2$} Using PHI Program

Simulations of the experimental plots χT(T) and M(H) for the binuclear complex {(hfac)$_2$Co^{II}(BN)Co^{II}(hfac)$_2$}, comprising four paramagnetic centers, were performed at a fixed value of $\lambda = -180$ cm^{-1} using both Set 1 and Set 2. However, as can be seen in Figure S3 (SM), none of the theoretical plots do not reproduce the experimental ones well. Therefore, an additional variation in the parameters is necessary to solve this problem.

Thus, we added the orbital reduction factor (σ) and zJ (mean field parameter) to a set of parameters to be varied when fitting the experimental magnetic behavior of the complex {(hfac)$_2$Co^{II}(BN)Co^{II}(hfac)$_2$}. The obtained extended Set1 and Set2 for the parameters of the spin–Hamiltonian (4) are presented in the bottom part of Table 3. The graphical results for fitting χT(T) and simulating M(H) using the extended parameter sets are shown in Figure 6. It should be noted that the approximation quality of the temperature curve χT(T) is almost the same for both sets. However, the corresponding simulation M(H) plot is still far from the experimental one, the obtained value of 0.07 for σ being unrealistically small. Hence, we took a slightly different approach. Instead of fitting χT(T) data, we performed the M(H) experimental data approximation by varying the parameters $B_2^{(0)}$, $B_2^{(2)}$, J_{CoN}, J_N, σ, and zJ for a set of λ values (−110, −130, −150 and −170 cm^{-1}). Figure 7 shows the χT(T) simulation for the optimal parameter set when $\lambda = -130$ cm^{-1} is fixed for the case $B_2^{(0)} > 0$. The optimal curves corresponding to the parameter set of $B_2^{(0)}$, $B_2^{(2)}$, J_{CoN}, J_N, and σ for other λ values (Table 3) look very similar and have a comparable approximation quality.

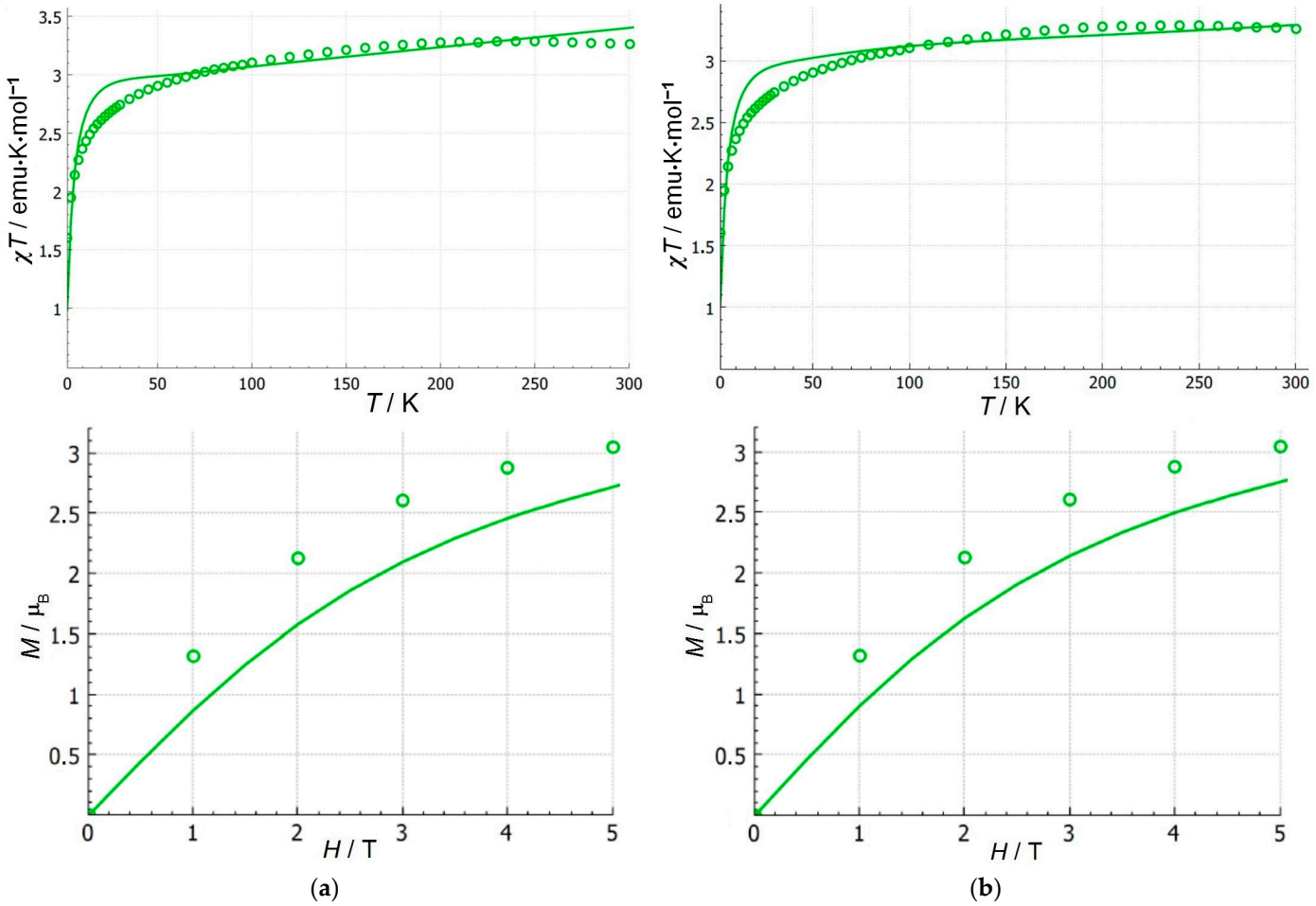

Figure 6. Simulations at $\lambda = -180$ cm^{-1} for the χT(T) and M(H) using the extended sets of spin–Hamiltonian parameters: (**a**) Set1 and (**b**) Set 2. Open circles are the experimental values.

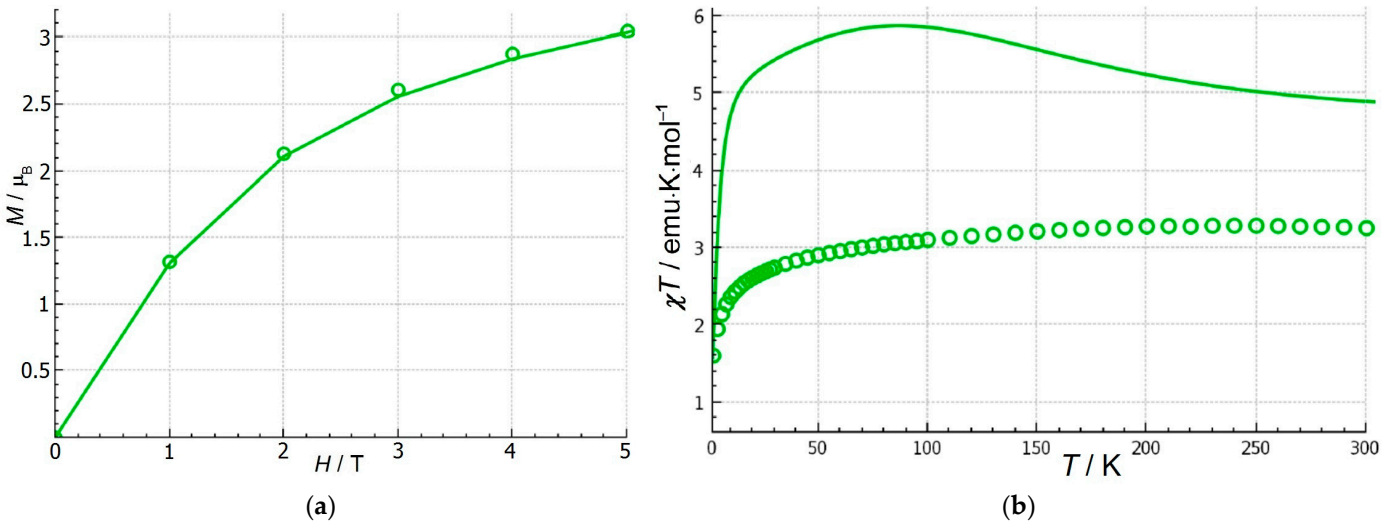

Figure 7. Simulations at $\lambda = -130$ cm^{-1} and $B_2^{(0)} > 0$ from Table 3 for (**a**) M(H) and (**b**) χT(T). Open circles are the experimental values.

To more accurately simulate the χT(T) behavior at low temperatures, a small average molecular field, zJ, was additionally introduced. The optimal values for zJ are given in the last column of Table 4. Figure 8 shows the final optimal approximation at $\lambda = -130$ cm^{-1}

and $zJ = -0.254$ cm^{-1}, which most closely reproduces the experimental χT(T) plot while giving reasonable values for the orbital reduction factor σ. It should also be noted that the optimal curves for the χT(T) dependence obtained at other values of the spin–orbit interaction parameter λ look graphically similar.

Table 4. Best parameters (in cm^{-1}) of the Hamiltonians (4), (3), and (2) for the cases when $B_2^{(0)} > 0$—upper part, and $B_2^{(0)} < 0$—lower part.

λ	$B_2^{(0)}$	$B_2^{(2)}$	σ [1]	J_{CoN}	J_N	zJ
−110	549	–205	–0.98	–93	−171	–0.328
−130 [2]	817 [2]	–265 [2]	–0.55 [2]	–62 [2]	−120 [2]	–0.254 [2]
−150	1012	–223	−1.14	–52	–77	–0.256
−170	1216	190	−1.4	–81	−156	–0.249
−110 [3]	−188 [3]	−11 [3]	−1.33 [3]	−121 [3]	–231 [3]	
−130	–236	−12	−1.38	−146	−192	
−150	–288	−12	−1.41	−161	−166	
−170	–357	−11	−1.4	−166	−162	

[1] Orbital reduction factor is a dimensionless quantity. [2,3] Set used for Figures 8 and 9, respectively. The parameter sets that best simulate the experimental magnetic dependences are highlighted in underlined text.

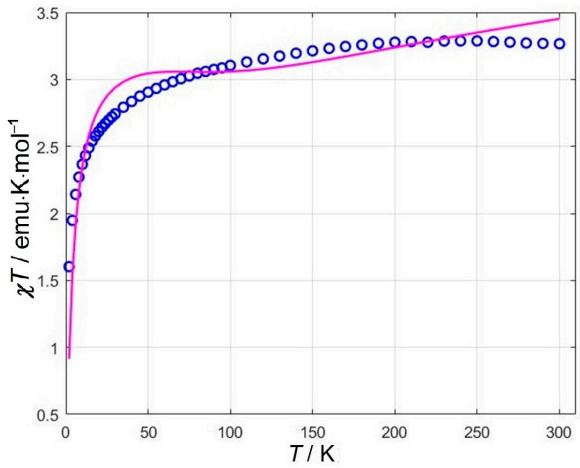

Figure 8. Final fit of χT(T) for $B_2^{(0)} > 0$ at $\lambda = -130$ cm^{-1} and $zJ = -0.254$ cm^{-1}, Table 4. Open circles are the experimental values.

An approximation of the field dependence M(H) was also performed for a few possible values of $B_2^{(0)} < 0$, resulting in the optimal parameters also shown in Table 4 (lower part). However, despite the good fitting quality for the M(H) dependence, a typical theoretical curve for χT(T) obtained with the parameter sets from Table 4 and $B_2^{(0)} < 0$ is far from the experimental one (Figure 9b). There is a clear difference between the theoretical and experimental values of χT(T). This discrepancy cannot be eliminated by adding any mean-field parameter zJ to the set of varying parameters in the fitting procedure. Thus, based on the approximation quality of the experimental data for χT(T) and M(H), the choice between the two values $B_2^{(0)} < 0$ and $B_2^{(0)} > 0$ was made in favor of the latter. However, there is still some uncertainty in the choice of an optimal value of λ. This fact makes it impossible to select an ideal set of parameters $B_2^{(0)}$, $B_2^{(2)}$, J_{CoN}, J_N, σ, zJ for a more accurate description of the magnetic behavior of the complex {(hfac)$_2$Co^{II}(BN)Co^{II}(hfac)$_2$}.

In summary, an analysis of the totality of experimental and theoretical data, both χT(T) and M(H), testifies that for the description of the magnetic behavior of {(hfac)$_2$Co^{II}(BN)Co^{II}(hfac)$_2$}, the sets of parameters of the spin–Hamiltonian (4) with positive values of $B_2^{(0)}$ are the most suitable (Table 4, upper part).

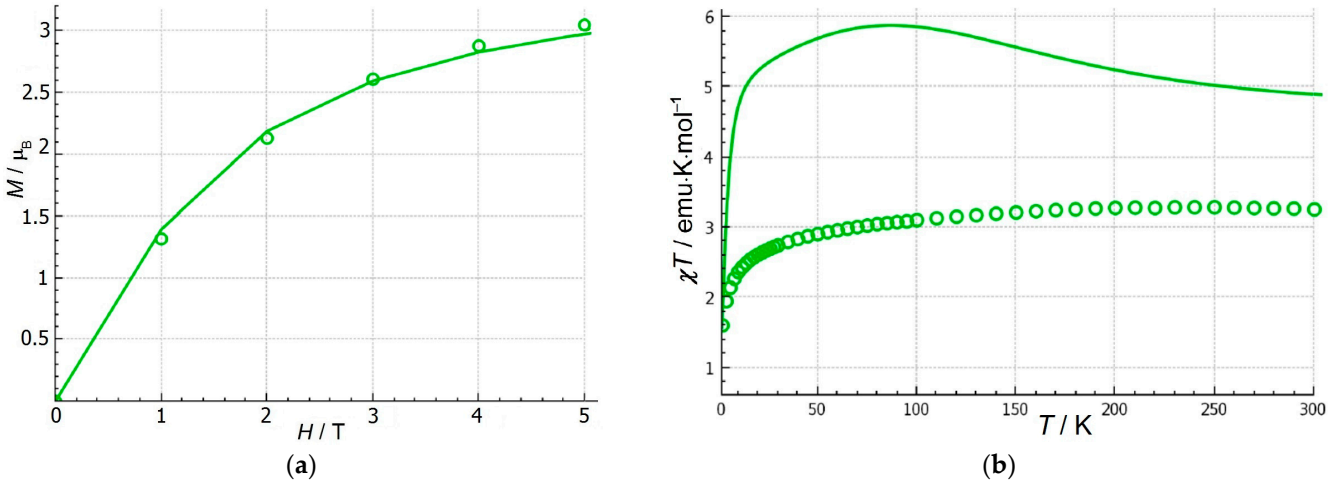

(**a**) (**b**)

Figure 9. A typical fit at $B_2^{(0)} < 0$ from Table 4 for (**a**) M(H) and (**b**) χT(T). Open circles are the experimental values.

In particular, depending on the value of the spin–orbit coupling in Co^{2+}, the exchange interaction J_N between the spins in the diradical BN varies from -77 to -171 cm^{-1}, while the magnetic exchange interaction of Co^{2+} with a monoradical of BN, J_{CoN}, varies from -52 to -93 cm^{-1}.

3.4.6. The Direct Ab Initio Calculation of Magnetic Dependences χT(T) and M(H)

The direct ab initio calculation of the magnetic dependences χT(T) and M(H) was carried out in the CAS(12,10)/def2-TZVP variant with finding 1, 5, 8, 8, and 5 roots for the multiplicities 9, 7, 5, 3, and 1 correspondingly. Such a choice of the number of roots for the multiplets (namely, their gradual increase in the preliminary calculations) was determined by taking into account all possible multiplets filling the energy range from 0 to 2000 cm^{-1}. As can be seen in Figure 10, the calculated plots χT(T) capture the main trends in the temperature dependence of the experimental χT(T) and also reproduce the experimental M(H) curve.

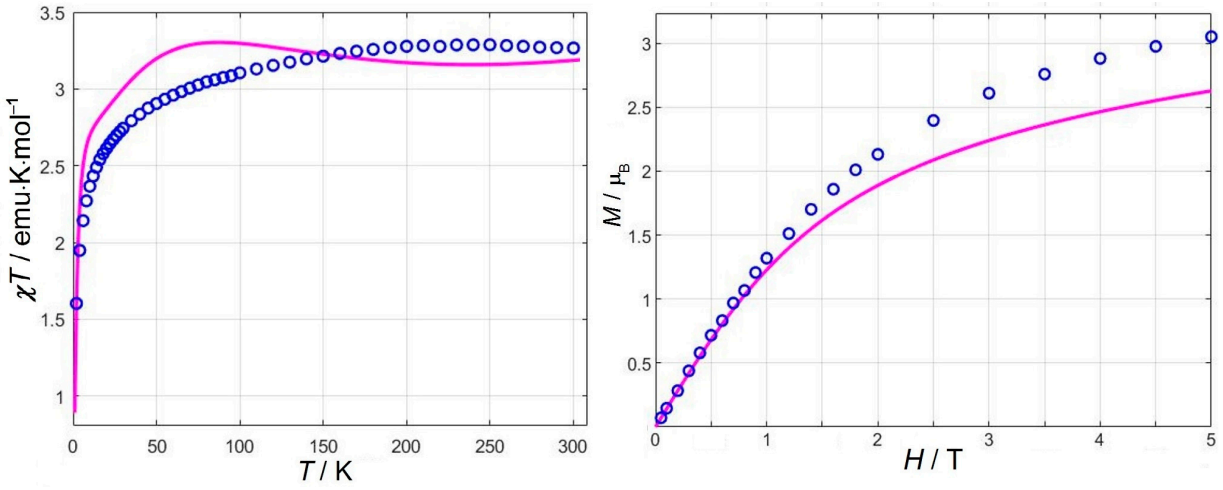

(**a**) (**b**)

Figure 10. Theoretical plots (solid lines) obtained from CAS(12,10)/def2-TZVPP calculation: (**a**) χT(T) and (**b**) M(H). Open circles are the experimental values.

4. Conclusions

By an improved and simplified procedure, a binuclear complex including high-spin Co^{2+} ions and a bridging bis-nitronyl nitroxyl radical, BN, was obtained for the first time. According to SCXRD, the complex $\{(hfac)_2Co^{II}(BN)Co^{II}(hfac)_2\}$ is isostructural to the previously studied congener $\{(hfac)_2Mn^{II}(BN)Mn^{II}(hfac)_2\}$.

The magnetic dependences of χT(T) and M(H) for the binuclear cobalt–diradical complex $\{(hfac)_2Co^{II}(BN)Co^{II}(hfac)_2\}$ have been analyzed in the formalism of the Griffith spin–Hamiltonian. It was clearly shown that for this magnetic system, only the case of positive values of the parameter $B_2^{(0)}$ takes place. This allowed us to determine the range of possible values for the magnetic exchange integral J_{CoN} between Co ions and NN radicals, as well as for the magnetic exchange integral J_N between monoradicals in BN. Assuming a frequently used value for the spin–orbit coupling parameter $\lambda \sim -170$ cm^{-1} [13], the values $J_{CoN} \sim -80$ cm^{-1} and $J_N \sim -160$ cm^{-1} could be obtained.

Supplementary Materials: The following supporting information can be downloaded at https://www.mdpi.com/article/10.3390/magnetochemistry10110082/s1, Table S1: Crystal data and single-crystal XRD experimental details; Figure S1: Powder X-Ray diffraction pattern of $\{(hfac)_2Co^{II}(BN)Co^{II}(hfac)_2\}$ measured at room temperature compared to the pattern simulated from the single crystal structure measured at 150 K; Figure S2: Field dependences of the normalized magnetizations measured at a sweep rate of 0.14 T s^{-1} at low temperatures from single crystals of $\{(hfac)_2Co^{II}(BN)Co^{II}(hfac)_2\}$; Table S2: The first 40 levels and their energy values for $\{(hfac)_2Co^{II}(BN)Co^{II}(hfac)_2\}$ obtained by ab initio calculations; Figure S3: The simulations at $\lambda = -180$ cm^{-1} for the χT(T) and M(H) using two different sets of spin–Hamiltonian parameters: (a) Set1 and (b) Set 2. Open circles are the experimental values.

Author Contributions: Conceptualization, K.E.V. and V.A.M.; methodology, K.E.V.; software, V.A.M.; validation, K.E.V., V.A.M. and E.V.P.; investigation, K.E.V., V.A.M., E.V.P. and W.W.; resources, K.E.V.; data curation, E.V.P. and W.W.; writing—original draft preparation, K.E.V., V.A.M. and E.V.P.; writing—review and editing, K.E.V., V.A.M., E.V.P. and W.W.; visualization, K.E.V., V.A.M., E.V.P. and W.W.; supervision, K.E.V. All authors have read and agreed to the published version of the manuscript.

Funding: This research was funded by the Ministry of Science and Higher Education of the Russian Federation, project No. 121031700313-3.

Data Availability Statement: Crystallographic data were deposited with the Cambridge Crystallographic Data Centre (deposit number CCDC 2366221). Copies of the data can be obtained free of charge via https://www.ccdc.cam.ac.uk/structures/ (accessed on 10 June 2024) (or from the Cambridge Crystallographic Data Centre, 12, Union Road, Cambridge, CB2 1EZ, UK; Fax: +44 1223 336033; e-mail: deposit@ccdc.cam.ac.uk).

Acknowledgments: We thank Checa Ruben for the magnetic data collection.

Conflicts of Interest: The authors declare no conflict of interest.

References

1. Caneschi, A.; Gatteschi, D.; Sessoli, R.; Rey, P. Toward Molecular Magnets: The Metal-Radical Approach. *Acc. Chem. Res.* **1989**, *22*, 392–398. [CrossRef]
2. Malrieu, J.P.; Caballol, R.; Calzado, C.J.; de Graaf, C.; Guihéry, N. Magnetic Interactions in Molecules and Highly Correlated Materials: Physical Content, Analytical Derivation, and Rigorous Extraction of Magnetic Hamiltonians. *Chem. Rev.* **2014**, *114*, 429–492. [CrossRef] [PubMed]
3. Caneschi, A.; Gatteschi, D.; Laugier, J.; Rey, P.; Sessoli, R.; Zanchini, C. Preparation, Crystal Structure, and Magnetic Properties of an Oligonuclear Complex with 12 Coupled Spins and an S = 12 Ground State. *J. Am. Chem. Soc.* **1988**, *110*, 2795–2799. [CrossRef]
4. Luneau, D.; Rey, P.; Laugier, J.; Belorizky, E.; Cogne, A. Ferromagnetic Behavior of Nickel(II)-Imino Nitroxide Derivatives. *Inorg. Chem.* **1992**, *31*, 3578–3584. [CrossRef]
5. Caneschi, A.; Gatteschi, D.; Laugier, J.; Rey, P. Ferromagnetic Alternating Spin Chains. *J. Am. Chem. Soc.* **1987**, *109*, 2191–2192. [CrossRef]
6. Caneschi, A.; Gatteschi, D.; Rey, P.; Sessoli, R. Structure and Magnetic Properties of Ferrimagnetic Chains Formed by Manganese(II) and Nitronyl Nitroxides. *Inorg. Chem.* **1988**, *27*, 1756–1761. [CrossRef]

7. Ovcharenko, V.I.; Vostrikova, K.E.; Ikorskii, V.N.; Larionov, S.V.; Sagdeev, R.Z. The Low Temperature Ferromagnet Dimethanol-Bis-[2,2,5,5-Tetramethyl-1-Oxyl-3-Imidazoline-4-(3′,3′,3′-Tri Fluoromethyl-1′-Propenyl-2′-Oxyato)] Cobalt(II), $CoL_2(CH_3OH)_2$. *Dokl. Akad. Nauk SSSR* **1989**, *306*, 660–662.
8. Vostrikova, K.E. High-Spin Molecules Based on Metal Complexes of Organic Free Radicals. *Coord. Chem. Rev.* **2008**, *252*, 1409–1419. [CrossRef]
9. Demir, S.; Jeon, I.-R.; Long, J.R.; Harris, T.D. Radical Ligand-Containing Single-Molecule Magnets. *Coord. Chem. Rev.* **2015**, *289–290*, 149–176. [CrossRef]
10. Shao, D.; Wang, X. Development of Single-Molecule Magnets. *Chin. J. Chem.* **2020**, *38*, 1005–1018. [CrossRef]
11. Liu, X.; Feng, X.; Meihaus, K.R.; Meng, X.; Zhang, Y.Y.-Q.Y.; Li, L.; Liu, J.J.-L.; Pedersen, K.S.; Keller, L.; Shi, W.; et al. Coercive Fields Above 6 T in Two Cobalt(II)–Radical Chain Compounds. *Angew. Chem. Int. Ed.* **2020**, *59*, 10610–10618. [CrossRef] [PubMed]
12. Meng, X.; Shi, W.; Cheng, P. Magnetism in One-Dimensional Metal–Nitronyl Nitroxide Radical System. *Coord. Chem. Rev.* **2019**, *378*, 134–150. [CrossRef]
13. Maryunina, K.; Nigomedyanova, D.; Morozov, V.; Smirnova, K.; Letyagin, G.; Romanenko, G.; Efimov, N.; Bogomyakov, A.; Ovcharenko, V. Ferrocenyl-Substituted Nitronyl Nitroxide in the Design of One-Dimensional Magnets. *Dalt. Trans.* **2024**, *53*, 1714–1721. [CrossRef]
14. Moreno-Pineda, E.; Wernsdorfer, W. Measuring Molecular Magnets for Quantum Technologies. *Nat. Rev. Phys.* **2021**, *3*, 645–659. [CrossRef]
15. Swain, A.; Sharma, T.; Rajaraman, G. Strategies to Quench Quantum Tunneling of Magnetization in Lanthanide Single Molecule Magnets. *Chem. Commun.* **2023**, *59*, 3206–3228. [CrossRef]
16. Kahn, O. *Molecular Magnetism*; VCH: New York, NY, USA, 1993; ISBN 978-1-56081-566-2.
17. Fujita, J.; Tanaka, M.; Suemune, H.; Koga, N.; Matsuda, K.; Iwamura, H. Antiferromagnetic Exchange Interaction among the Three Spins Placed in an Isosceles Triangular Configuration in 2,4-Dimethoxy-1,3,5-Benzenetriyltris(N-Tert-Butyl Nitroxide). *J. Am. Chem. Soc.* **1996**, *118*, 9347–9351. [CrossRef]
18. Furui, T.; Suzuki, S.; Kozaki, M.; Shiomi, D.; Sato, K.; Takui, T.; Okada, K.; Tretyakov, E.V.; Tolstikov, S.E.; Romanenko, G.V.; et al. Preparation and Magnetic Properties of Metal-Complexes from N-t-Butyl-N-Oxidanyl-2-Amino-(Nitronyl Nitroxide). *Inorg. Chem.* **2014**, *53*, 802–809. [CrossRef]
19. Barclay, T.M.; Hicks, R.G.; Lemaire, M.T.; Thompson, L.K. Synthesis, Structure, and Magnetism of Bimetallic Manganese or Nickel Complexes of a Bridging Verdazyl Radical. *Inorg. Chem.* **2001**, *40*, 5581–5584. [CrossRef]
20. Wang, J.; Li, J.-N.; Zhang, S.-L.; Zhao, X.-H.; Shao, D.; Wang, X.-Y. Syntheses and Magnetic Properties of a Pyrimidyl-Substituted Nitronyl Nitroxide Radical and Its Cobalt(II) Complexes. *Chem. Commun.* **2016**, *52*, 5033–5036. [CrossRef]
21. Xia, C.-C.; Zhang, X.-Y.; Zhang, C.-C.; Li, G.; Wei, H.-Y.; Wang, X.-Y. Syntheses and Magnetic Properties of a Bis-Bidentate Nitronyl Nitroxide Radical Based on Triazolopyrimidine and Its Metal Complexes. *Dalt. Trans.* **2023**, *52*, 8964–8974. [CrossRef]
22. Caneschi, A.; Gatteschi, D.; Rey, P. The Chemistry and Magnetic Properties of Metal Nitronyl Nitroxide Complexes. In *Progress in Inorganic Chemistry*; Lippard, S.J., Ed.; John Wiley & Sons, Inc.: New York, NY, USA, 1991; pp. 331–429. ISBN 9780470166406.
23. Yoshioka, N.; Irisawa, M.; Mochizuki, Y.; Kato, T.; Inoue, H.; Ohba, S. Unusually Large Magnetic Interactions Observed in Hydrogen-Bonded Nitronyl Nitroxides. *Chem. Lett.* **1997**, *26*, 251–252. [CrossRef]
24. Iwamura, H.; Inoue, K.; Hayamizu, T. High-Spin Polynitroxide Radicals as Versatile Bridging Ligands for Transition Metal Complexes with High Ferri/Ferromagnetic Tc. *Pure Appl. Chem.* **1996**, *68*, 243–252. [CrossRef]
25. Luneau, D.; Laugier, J.; Rey, P.; Ulrich, G.; Ziessel, R.; Legoll, P.; Drillon, M. Synthesis, Coordination and Magnetic Properties of a Novel Family of Stable Chelate Based Biradicals: Molecular Structure of a 2,2′-Bipyridine N-Oxide N-Oxyl Biradical and Its Copper(II) Complex. *J. Chem. Soc. Chem. Commun.* **1994**, *6*, 741–742. [CrossRef]
26. Sanfui, S.; Usman, M.; Roychowdhury, A.; Pramanik, S.; Garribba, E.; Gómez García, C.J.; Chen, P.P.-Y.; Rath, S.P. Bridge vs Terminal Cyano-Coordination in Binuclear Cobalt Porphyrin Dimers: Interplay of Electrons between Metal and Ligand and Spin-Coupling via Bridge. *Inorg. Chem.* **2024**, *63*, 15619–15633. [CrossRef]
27. Titiš, J.; Rajnák, C.; Boča, R. Magnetostructural D-Correlations and Their Impact on Single-Molecule Magnetism. *Inorganics* **2023**, *11*, 452. [CrossRef]
28. Sakamoto, A.; Harada, T.; Tonegawa, N. A New Approach to the Spectral Study of Unstable Radicals and Ions in Solution by the Use of an Inert Gas Glovebox System: Observation and Analysis of the Infrared Spectra of the Radical Anion and Dianion of p-Terphenyl. *J. Phys. Chem. A* **2008**, *112*, 1180–1187. [CrossRef]
29. Audier, H.E.; Milliet, A.; Leblanc, D.; Morton, T.H. Unimolecular Decompositions of the Radical Cations of Ethylene Glycol and Its Monomethyl Ether in the Gas Phase. Distonic Ions versus Ion-Neutral Complexes. *J. Am. Chem. Soc.* **1992**, *114*, 2020–2027. [CrossRef]
30. Luneau, D.; Rey, P. Magnetism of Metal-Nitroxide Compounds Involving Bis-Chelating Imidazole and Benzimidazole Substituted Nitronyl Nitroxide Free Radicals. *Coord. Chem. Rev.* **2005**, *249*, 2591–2611. [CrossRef]
31. Vaz, M.G.F.; Andruh, M. Molecule-Based Magnetic Materials Constructed from Paramagnetic Organic Ligands and Two Different Metal Ions. *Coord. Chem. Rev.* **2021**, *427*, 213611. [CrossRef]
32. Luneau, D. Coordination Chemistry of Nitronyl Nitroxide Radicals Has Memory. *Eur. J. Inorg. Chem.* **2020**, *2020*, 597–604. [CrossRef]

33. Ullman, E.F.; Boocock, D.G.B. "Conjugated" Nitronyl-Nitroxide and Imino-Nitroxide Biradicals. *J. Chem. Soc. D Chem. Commun.* **1969**, *20*, 1161–1162. [CrossRef]
34. Alies, F.; Luneau, D.; Laugier, J.; Rey, P. Ullmann's Nitroxide Biradicals Revisited. Structural and Magnetic Properties. *J. Phys. Chem.* **1993**, *97*, 2922–2925. [CrossRef]
35. Maekawa, K.; Shiomi, D.; Ise, T.; Sato, K.; Takui, T. Experimental Evidence for the Triplet-Like Spin State Appearing in Ground-State Singlet Biradicals as a Key Feature for Generalized Ferrimagnetic Spin Alignment. *J. Phys. Chem. B* **2006**, *110*, 2102–2107. [CrossRef]
36. Tanaka, M.; Matsuda, K.; Itoh, T.; Iwamura, H. A Spin-Frustrated System Composed of Organic Radicals and Magnetic Metal Ions. *Angew. Chem. Int. Ed.* **1998**, *37*, 810–812. [CrossRef]
37. Bain, G.A.; Berry, J.F. Diamagnetic Corrections and Pascal's Constants. *J. Chem. Educ.* **2008**, *85*, 532. [CrossRef]
38. Wernsdorfer, W. Classical and Quantum Magnetization Reversal Studied in Nanometer-Sized Particles and Clusters. In *Advances in Chemical Physics*; Wiley: Hoboken, NJ, USA, 2001; pp. 99–190. ISBN 9780470141786. [CrossRef]
39. Shoji, M.; Koizumi, K.; Kitagawa, Y.; Kawakami, T.; Yamanaka, S.; Okumura, M.; Yamaguchi, K. A General Algorithm for Calculation of Heisenberg Exchange Integrals J in Multispin Systems. *Chem. Phys. Lett.* **2006**, *432*, 343–347. [CrossRef]
40. Neese, F.; Wennmohs, F.; Becker, U.; Riplinger, C. The ORCA Quantum Chemistry Program Package. *J. Chem. Phys.* **2020**, *152*, 224108. [CrossRef]
41. Neese, F. Software Update: The ORCA Program System—Version 5.0. *WIREs Comput. Mol. Sci.* **2022**, *12*, e1606. [CrossRef]
42. Chilton, N.F.; Anderson, R.P.; Turner, L.D.; Soncini, A.; Murray, K.S. PHI: A Powerful New Program for the Analysis of Anisotropic Monomeric and Exchange-coupled Polynuclear d- and f-block Complexes. *J. Comput. Chem.* **2013**, *34*, 1164–1175. [CrossRef]
43. Tominaga, T.; Mochida, T. Trans-Diaquabis(1,1,1,5,5,5-Hexafluoropentane-2,4-Dionato-κ 2O,O′)Cobalt(II) Dihydrate. *IUCrData* **2017**, *2*, x170002. [CrossRef]
44. Catala, L.; Wurst, K.; Amabilino, D.B.; Veciana, J. Polymorphs of a Pyrazole Nitronyl Nitroxide and Its Complexes with Metal(Ii) Hexafluoroacetylacetonates. *J. Mater. Chem.* **2006**, *16*, 2736. [CrossRef]
45. Vostrikova, K.E.; Belorizky, E.; Pécaut, J.; Rey, P. New Chelating Nitroxide Free Radical Ligands for Heterospin-Magnetic Engineering. *Eur. J. Inorg. Chem.* **1999**, *7*, 1181–1187. [CrossRef]
46. Ostrovsky, S.M.; Falk, K.; Pelikan, J.; Brown, D.A.; Tomkowicz, Z.; Haase, W. Orbital Angular Momentum Contribution to the Magneto-Optical Behavior of a Binuclear Cobalt(II) Complex. *Inorg. Chem.* **2006**, *45*, 688–694. [CrossRef] [PubMed]
47. Boeer, A.B.; Barra, A.-L.; Chibotaru, L.F.; Collison, D.; McInnes, E.J.L.; Mole, R.A.; Simeoni, G.G.; Timco, G.A.; Ungur, L.; Unruh, T.; et al. A Spectroscopic Investigation of Magnetic Exchange Between Highly Anisotropic Spin Centers. *Angew. Chem. Int. Ed.* **2011**, *50*, 4007–4011. [CrossRef]
48. Zorina, E.N.; Zauzolkova, N.V.; Sidorov, A.A.; Aleksandrov, G.G.; Lermontov, A.S.; Kiskin, M.A.; Bogomyakov, A.S.; Mironov, V.S.; Novotortsev, V.M.; Eremenko, I.L. Novel Polynuclear Architectures Incorporating Co^{2+} and K^{+} Ions Bound by Dimethylmalonate Anions: Synthesis, Structure, and Magnetic Properties. *Inorg. Chim. Acta* **2013**, *396*, 108–118. [CrossRef]
49. Domínguez, S.; Mederos, A.; Gili, P.; Rancel, A.; Rivero, A.E.; Brito, F.; Lloret, F.; Solans, X.; Ruíz-Pérez, C.; Rodríguez, M.L.; et al. Dimer Complexes of 2,4-Toluenediamine-N,N,N′,N′-Tetraacetic Acid (2,4-TDTA) with Copper(II), Nickel(II), Cobalt(II), Zinc(II) and Manganese(II). Studies in Aqueous Solution and Solid State. X-Ray Crystal Structures of $Na_4[Ni_2(2,4\text{-}TDTA)_2]\cdot 15H_2O$ and $Na_4[Cu_2(2,4\text{-}TDTA)_2]\cdot 20H_2O$. *Inorg. Chim. Acta* **1997**, *255*, 367–380. [CrossRef]
50. Sakiyama, H.; Ito, R.; Kumagai, H.; Inoue, K.; Sakamoto, M.; Nishida, Y.; Yamasaki, M. Dinuclear Cobalt(II) Complexes of an Acyclic Phenol-Based Dinucleating Ligand with Four Methoxyethyl Chelating Arms—First Magnetic Analyses in an Axially Distorted Octahedral Field. *Eur. J. Inorg. Chem.* **2001**, *2001*, 2027–2032. [CrossRef]
51. Clemente, J.M.; Andres, H.; Aebersold, M.; Borrás-Almenar, J.J.; Coronado, E.; Güdel, H.U.; Büttner, H.; Kearly, G. Magnetic Excitations in Tetrameric Clusters of Polyoxometalates Observed by Inelastic Neutron Scattering. Evidence for Anisotropic Exchange Interactions in Cobalt(II) Clusters. *Inorg. Chem.* **1997**, *36*, 2244–2245. [CrossRef]
52. Hossain, M.J.; Yamasaki, M.; Mikuriya, M.; Kuribayashi, A.; Sakiyama, H. Synthesis, Structure, and Magnetic Properties of Dinuclear Cobalt(II) Complexes with a New Phenol-Based Dinucleating Ligand with Four Hydroxyethyl Chelating Arms. *Inorg. Chem.* **2002**, *41*, 4058–4062. [CrossRef]
53. Griffith, J.S. *The Theory of Transition Metal Ions*; Reissue; University Press: Cambridge, UK, 2009; ISBN 978-0521115995.
54. Figgis, B.N. *Introduction to Ligand Fields*; John Wiley & Sons Ltd., Interscience Publication: London, UK; New York, NY, USA, 1966; ISBN 9780898748192.
55. Palii, A.V.; Korchagin, D.V.; Yureva, E.A.; Akimov, A.V.; Misochko, E.Y.; Shilov, G.V.; Talantsev, A.D.; Morgunov, R.B.; Aldoshin, S.M.; Tsukerblat, B.S. Single-Ion Magnet $Et_4N[Co^{II}(Hfac)_3]$ with Nonuniaxial Anisotropy: Synthesis, Experimental Characterization, and Theoretical Modeling. *Inorg. Chem.* **2016**, *55*, 9696–9706. [CrossRef]